

# Voltage-Gated Ion Channels in Human Pancreatic $\beta$ -Cells: Electrophysiological Characterization and Role in Insulin Secretion

Matthias Braun,<sup>1</sup> Reshma Ramracheya,<sup>1</sup> Martin Bengtsson,<sup>1</sup> Quan Zhang,<sup>1</sup> Jovita Karanauskaite,<sup>1</sup> Chris Partridge,<sup>1</sup> Paul R. Johnson,<sup>2</sup> and Patrik Rorsman<sup>1</sup>

**OBJECTIVE**—To characterize the voltage-gated ion channels in human  $\beta$ -cells from nondiabetic donors and their role in glucose-stimulated insulin release.

**RESEARCH DESIGN AND METHODS**—Insulin release was measured from intact islets. Whole-cell patch-clamp experiments and measurements of cell capacitance were performed on isolated  $\beta$ -cells. The ion channel complement was determined by quantitative PCR.

**RESULTS**—Human  $\beta$ -cells express two types of voltage-gated  $K^+$  currents that flow through delayed rectifying ( $K_v2.1/2.2$ ) and large-conductance  $Ca^{2+}$ -activated  $K^+$  (BK) channels. Blockade of BK channels (using iberiotoxin) increased action potential amplitude and enhanced insulin secretion by 70%, whereas inhibition of  $K_v2.1/2.2$  (with stromatotoxin) was without stimulatory effect on electrical activity and secretion. Voltage-gated tetrodotoxin (TTX)-sensitive  $Na^+$  currents ( $Na_v1.6/1.7$ ) contribute to the upstroke of action potentials. Inhibition of  $Na^+$  currents with TTX reduced glucose-stimulated (6–20 mmol/l) insulin secretion by 55–70%. Human  $\beta$ -cells are equipped with L- ( $Ca_v1.3$ ), P/Q- ( $Ca_v2.1$ ), and T- ( $Ca_v3.2$ ), but not N- or R-type  $Ca^{2+}$  channels. Blockade of L-type channels abolished glucose-stimulated insulin release, while inhibition of T- and P/Q-type  $Ca^{2+}$  channels reduced glucose-induced (6 mmol/l) secretion by 60–70%. Membrane potential recordings suggest that L- and T-type  $Ca^{2+}$  channels participate in action potential generation. Blockade of P/Q-type  $Ca^{2+}$  channels suppressed exocytosis (measured as an increase in cell capacitance) by >80%, whereas inhibition of L-type  $Ca^{2+}$  channels only had a minor effect.

**CONCLUSIONS**—Voltage-gated T-type and L-type  $Ca^{2+}$  channels as well as  $Na^+$  channels participate in glucose-stimulated electrical activity and insulin secretion.  $Ca^{2+}$ -activated BK channels are required for rapid membrane repolarization. Exocytosis of insulin-containing granules is principally triggered by  $Ca^{2+}$  influx through P/Q-type  $Ca^{2+}$  channels. *Diabetes* 57:1618–1628, 2008

From the <sup>1</sup>Oxford Centre for Diabetes Endocrinology and Metabolism, University of Oxford, Churchill Hospital, Oxford, U.K.; and the <sup>2</sup>Nuffield Department of Surgery, John Radcliffe Hospital, Oxford, U.K.

Corresponding author: Matthias Braun, Oxford Centre for Diabetes, Endocrinology, and Metabolism, Churchill Hospital, Old Road, Oxford OX37 LJ, U.K. E-mail: matthias.braun@drl.ox.ac.uk

Received for publication 17 July 2007 and accepted in revised form 13 March 2008.

Published ahead of print at <http://diabetes.diabetesjournals.org> on 17 March 2008. DOI: 10.2337/db07-0991.

M.B. and R.R. contributed equally to this article.

Additional information for this article can be found in an online appendix at <http://dx.doi.org/10.2337/db07-0991>.

BK,  $Ca^{2+}$ -activated  $K^+$ ; IbTX, iberiotoxin; I-V, current-voltage relationship;  $K_{ATP}$  channel, ATP-sensitive  $K^+$  channel; TEA, tetraethylammonium; TTX, tetrodotoxin.

© 2008 by the American Diabetes Association.

The costs of publication of this article were defrayed in part by the payment of page charges. This article must therefore be hereby marked "advertisement" in accordance with 18 U.S.C. Section 1734 solely to indicate this fact.

Voltage-gated plasmalemmal ion channels play a fundamental role in stimulus secretion coupling in  $\beta$ -cells, and  $Ca^{2+}$  influx through voltage-gated  $Ca^{2+}$  channels triggers exocytosis of insulin-containing secretory granules (1). Voltage-gated  $Ca^{2+}$  channels are activated by coordinated fluctuations of the cell membrane potential (electrical activity), which are initiated by the glucose-induced closure of ATP-sensitive  $K^+$  channels ( $K_{ATP}$  channels) (2,3) and dependent on voltage-gated  $Na^+$  and  $K^+$  channels (4). Due to the limited availability of human islets, few electrophysiological studies of voltage-gated ion channels in human  $\beta$ -cells have been published, and the identity of the  $\beta$ -cells was not unequivocally established (5–8), although 45% of normal human islets cells are non- $\beta$ -cells (9). In some earlier studies (10–12), identification of  $\beta$ -cells was based on the presence of  $K_{ATP}$  currents. However, this is not unproblematic, as  $K_{ATP}$  channels are also found in non- $\beta$ -cells (13,14).

In the present study, we have identified the voltage-gated ion channels expressed in human  $\beta$ -cells obtained from nondiabetic donors and characterized their role in glucose-induced insulin secretion. Our data illustrate that human  $\beta$ -cells differ from rodent cells in several important respects.

## RESEARCH DESIGN AND METHODS

**Islet isolation and cell culture.** With appropriate ethical approval and clinical consent, pancreatic islets were isolated in the Diabetes Research and Wellness Foundation Human Islet Isolation Facility from human pancreata retrieved from nondiabetic, heart-beating donors. This study is based on 34 islet preparations. For patch-clamp experiments, islets were dispersed into single cells immediately after preparation by incubation in  $Ca^{2+}$ -free buffer followed by trituration. The cells were cultured in RPMI-1640 medium containing 10 mmol/l glucose and 2 mmol/l L-glutamine.

**Materials.**  $\omega$ -Conotoxin GVIA, SNX482,  $\omega$ -agatoxin IVA, and stromatotoxin-1 were purchased from Alomone Labs (Jerusalem, Israel) or the Peptide Institute (Osaka, Japan). Iberiotoxin (IbTX) was from Bachem (St. Helens, U.K.). All other chemicals were purchased from Sigma-Aldrich.

**Insulin secretion.** Insulin secretion was measured as described elsewhere (15). Briefly, batches of 10–20 islets (in triplicates) were preincubated in 1 ml Krebs-Ringer buffer supplemented with 1 mmol/l glucose for 1 h followed by a 1-h incubation in 1 ml of test Krebs-Ringer buffer medium supplemented as indicated.

**Electrophysiology.** Patch-clamp experiments were performed using an EPC-9 amplifier and Pulse software (HEKA, Lamprecht, Germany). All electrophysiological experiments were performed at 32–33°C using the standard or perforated-patch whole-cell configurations.

**Solutions.**  $K^+$  currents were recorded in an extracellular solution composed of (mmol/l) 138 NaCl, 5.6 KCl, 2.6  $CaCl_2$ , 1.2  $MgCl_2$ , 5 HEPES, and 5 glucose (pH 7.4, adjusted with NaOH). For recording  $Na^+$  and  $Ca^{2+}$  currents, 10 mmol/l tetraethylammonium (TEA) was added and NaCl correspondingly reduced. For  $Ca^{2+}$  current measurements, 0.1  $\mu$ g/ml tetrodotoxin was added

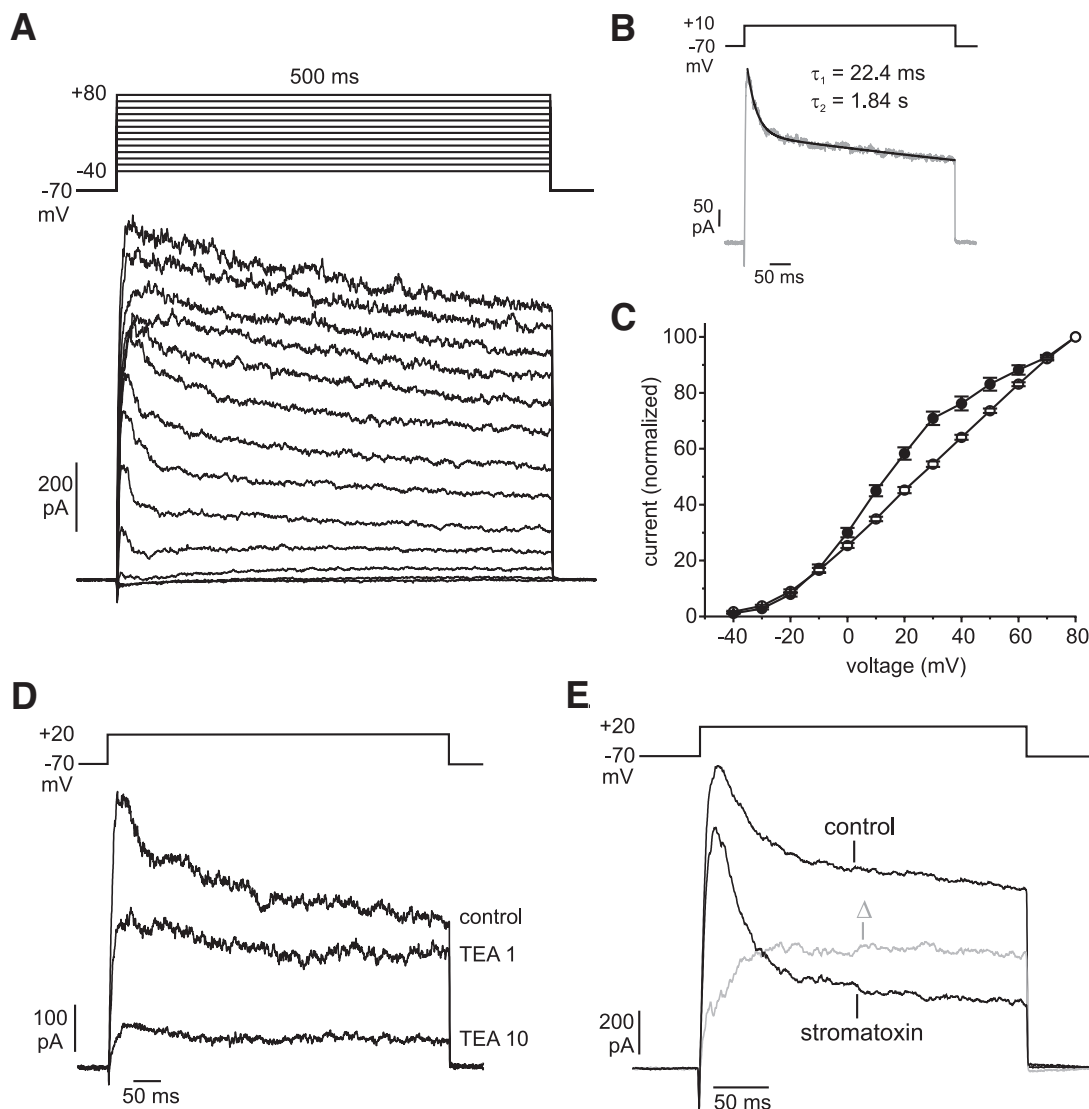


**FIG. 1.** Voltage-gated  $K^+$  currents in  $\beta$ -cells. **A:**  $K^+$  currents recorded during depolarizations to potentials between  $-40$  and  $+80$  mV (in  $10$ -mV steps). **B:** An exponential fit of the current decay using the time constants ( $\tau$ ) shown is superimposed on the current (same experiment as **A**). **C:** I-V relationship for peak ( $\bullet$ ) and sustained ( $\circ$ ) (measured at the end of  $500$ -ms depolarizations) current ( $n = 23$ ). The currents are expressed as percent of the responses at  $+80$  mV. **D:** Voltage-gated  $K^+$  currents recorded under control conditions and in the presence of  $1$  or  $10$  mmol/l TEA. **E:** Voltage-gated  $K^+$  currents recorded in the absence and presence of  $100$  nmol/l stromatoxin. The gray trace represents the difference current ( $\Delta$ ).

additionally. For  $Na^+$  current recordings, extracellular  $CaCl_2$  was replaced equimolarly with  $MgCl_2$  and  $1$  mmol/l  $CoCl_2$  included in the medium.

The intracellular solution for  $K^+$  current measurements contained (mmol/l)  $120$  KCl,  $1$   $MgCl_2$ ,  $10$  EGTA,  $1$   $CaCl_2$ ,  $10$  HEPES, and  $3$  MgATP (pH  $7.2$ , KOH).  $Na^+$  and  $Ca^{2+}$  current measurements were made after equimolar substitution of KCl by CsCl. For capacitance measurements, the pipette solution contained (mmol/l)  $125$  Cs-glutamate,  $10$  CsCl,  $10$  NaCl,  $1$   $MgCl_2$ ,  $5$  HEPES,  $0.05$  EGTA,  $3$  MgATP, and  $0.1$  cAMP (pH  $7.2$ , CsOH). Glucose- and tolbutamide-induced electrical activity was recorded in the perforated-patch whole-cell configuration as previously reported (16). Biotin ( $0.5$  mg/ml; Invitrogen) was added to all pipette solutions to facilitate subsequent establishment of cell identity.

**Immunocytochemistry.** Immunolabeling with antibodies against insulin, glucagon, and somatostatin and detection of biocytin-loaded cells was performed essentially as described previously (17).

**Quantitative RT-PCR.** Gene expression profiling of ion-channel isoforms was performed by RT-qPCR on human islet total RNA (for details see the online appendix [available at <http://dx.doi.org/10.2337/db07-0991>]).

**Data analysis.** All data points are expressed as means  $\pm$  SE of indicated number of experiments. All experiments were performed using islets/cells from at least two different donors. Inhibitory effects of channel blockers on glucose-induced insulin secretion are given after subtraction of basal release. Statistical significance was evaluated using Student's  $t$  test. A more detailed description of the experimental procedures is provided in the online appendix.

## RESULTS

**Voltage-gated  $K^+$  currents.** The identity of all  $\beta$ -cells used for electrophysiological analysis in this study was confirmed by immunocytochemistry. Human  $\beta$ -cells thus identified had a membrane capacitance ( $C_{slow}$ ) of  $9.9 \pm 0.3$  pF ( $n = 207$ ) (online appendix Fig. 1).

Voltage-gated  $K^+$  currents were elicited by  $500$  ms voltage-clamp depolarizations from a holding potential of  $-70$  mV. Outward  $K^+$  currents became detectable during depolarizations to  $-30$  mV and beyond (Fig. 1A). The activation kinetics of the  $K^+$  current elicited by depolarization to  $+10$  mV was estimated using a Hodgkin-Huxley  $m^4$  model. The time constant ( $\tau$ ) of activation averaged  $1.9 \pm 0.1$  ms ( $n = 31$ ). In  $26$  of  $31$  cells, current inactivation was best described as the sum of two exponentials (Fig. 1B). The average time constants ( $\tau$ ) were  $41 \pm 7$  ms for the fast (transient) component and  $1.8 \pm 0.1$  s for the slowly inactivating (sustained) current. The transient component accounted for  $28 \pm 2\%$  of the total current amplitude at

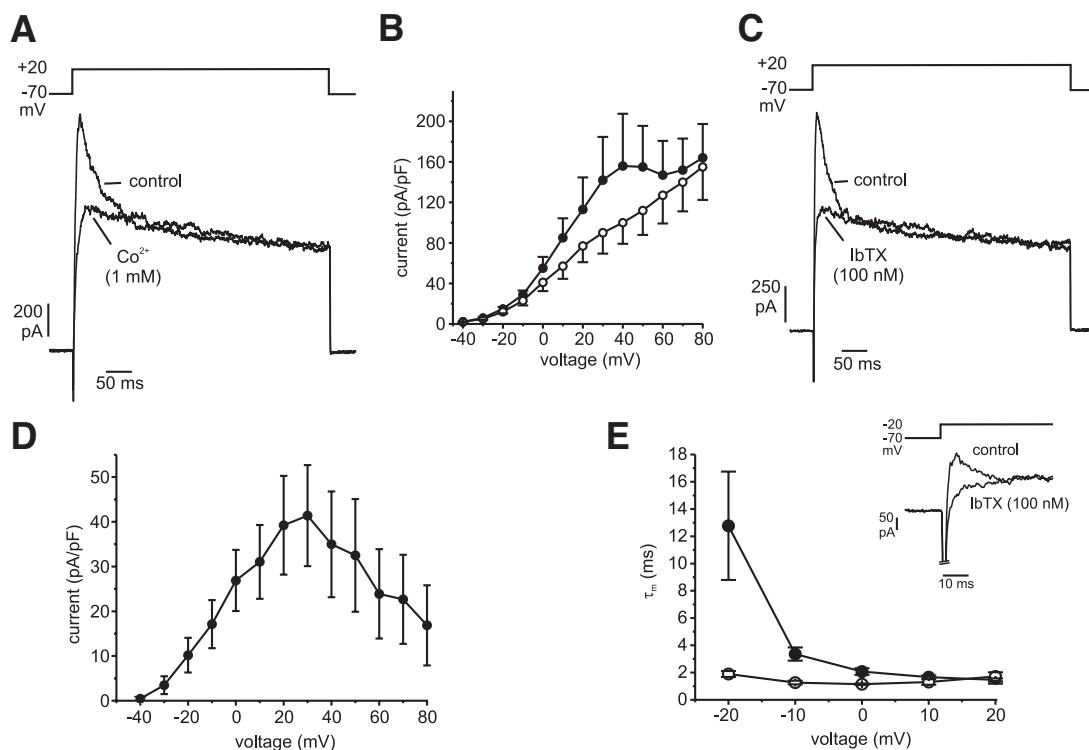


**FIG. 2.** Effects of  $\text{Co}^{2+}$  and IbTX on  $\text{K}^+$  currents. **A:**  $\text{K}^+$  currents recorded in the absence or presence of  $\text{Co}^{2+}$ . **B:** I-V relationship for peak outward currents (normalized to cell size) recorded in the absence ( $\bullet$ ) and presence ( $\circ$ ) of  $\text{Co}^{2+}$  ( $n = 3$ ). **C:**  $\text{K}^+$  currents recorded in the absence or presence of IbTX. **D:** I-V relationship of the IbTX-sensitive current ( $n = 9$ ). **E:** Voltage dependence of the activation time constants  $\tau_m$  of the IbTX-resistant ( $\bullet$ ) and -sensitive ( $\circ$ ) currents ( $n = 7$ ). *Inset* shows currents evoked by depolarizations to  $-20$  mV before and after application of IbTX on an expanded time base.

+10 mV. In the remaining five cells, the inactivation could be well described using a single time constant of  $1.8 \pm 0.3$  s. In cells with a transient current component, a small “shoulder” in the current-voltage relationship (I-V) relationship was apparent at voltages between +40 and +60 mV (Fig. 1A and C).

The peak outward current was sensitive to TEA; 1 and 10 mmol/l of this broad-spectrum  $\text{K}^+$  channel blocker inhibited  $50 \pm 3\%$  ( $n = 9$ ) and  $83 \pm 3\%$  ( $n = 14$ ), respectively (Fig. 1D). The  $\text{Kv}2.1/2.2$  antagonist stromatocytin-1 selectively inhibited the slowly inactivating outward current (Fig. 1E). In a series of eight experiments, the sustained current component (measured at the end of a 250-ms depolarization to +20 mV) was reduced by  $45 \pm 6\%$  ( $P < 0.001$ ), while the peak current decreased only by  $15 \pm 4\%$  ( $P < 0.01$ ).

The  $\text{Ca}^{2+}$  channel blocker  $\text{Co}^{2+}$  selectively abolished the transient current (Fig. 2A) and removed the shoulder in the I-V relationship (Fig. 2B). IbTX, a specific blocker of large-conductance  $\text{Ca}^{2+}$ -activated  $\text{K}^+$  channels (BK channels), also selectively blocked the transient  $\text{K}^+$  current (Fig. 2C), and its effect was indistinguishable from that of  $\text{Co}^{2+}$  (compare Fig. 2A and C). The IbTX-sensitive current was reconstructed by subtracting the current obtained in the presence of the blocker from that measured under control conditions. The isolated IbTX-sensitive current exhibited a bell-shaped voltage dependence with a peak of  $41 \pm 11$  pA/pF ( $n = 9$ ) at +30 mV (Fig. 2D), comparable with the  $52 \pm 23$  pA/pF ( $n = 3$ ) of the  $\text{Co}^{2+}$ -sensitive current (not shown).

Figure 2E (*inset*) shows the total and IbTX-resistant currents evoked by depolarization to  $-20$  mV. Whereas the current before IbTX activated rapidly, the IbTX-insen-

sitive current developed more slowly. Figure 2E summarizes the relationship between voltage and time constants of activation ( $\tau_m$ ) of IbTX-sensitive and -resistant currents. The IbTX-sensitive and -insensitive currents elicited by depolarizations to +10 mV inactivated with time constants of  $22 \pm 6$  ms ( $n = 7$ ) and  $1.6 \pm 0.3$  s ( $n = 7$ ), respectively (not shown). These values are comparable with the time constants for the fast and slowly inactivating components under control conditions described above. The magnitude of the IbTX-sensitive component at +10 mV was  $\sim 50\%$  of that of the IbTX-insensitive component (approximately one-third of the total), in good agreement with the fraction of the current showing rapid inactivation under control conditions (28%, see above).

The effects of the  $\text{K}^+$  channel blockers on  $\beta$ -cell electrical activity are shown in Fig. 3. TEA (10–20 mmol/l) increased the peak voltage of the action potentials induced by 6 mmol/l glucose ( $n = 3$ ) (Fig. 3A) or tolbutamide (100  $\mu\text{mol/l}$ ;  $n = 4$ ) from  $-13 \pm 5$  mV to  $4 \pm 7$  mV. The  $\text{Kv}2.1/2.2$  blocker stromatocytin had weak effects on electrical activity; a significant increase in spike height was observed in only one of seven cells (Fig. 3B) and the action potentials peaked at  $-21 \pm 3$  mV in both the absence and presence of the blocker ( $n = 4$  for glucose,  $n = 3$  for tolbutamide). Addition of IbTX significantly increased the amplitude of glucose-induced action potentials in two of five cells (Fig. 3C), whereas action potential firing was inhibited in the remaining three cells. The latter effect was accompanied by hyperpolarization and an increase in resting membrane conductance ( $n = 2$ ) (not shown), presumably reflecting activation of  $\text{K}_{\text{ATP}}$  channels. When IbTX was tested in the presence of tolbutamide (100  $\mu\text{mol/l}$ ), it consistently increased the amplitude of action potentials ( $n = 3$ ). Similar

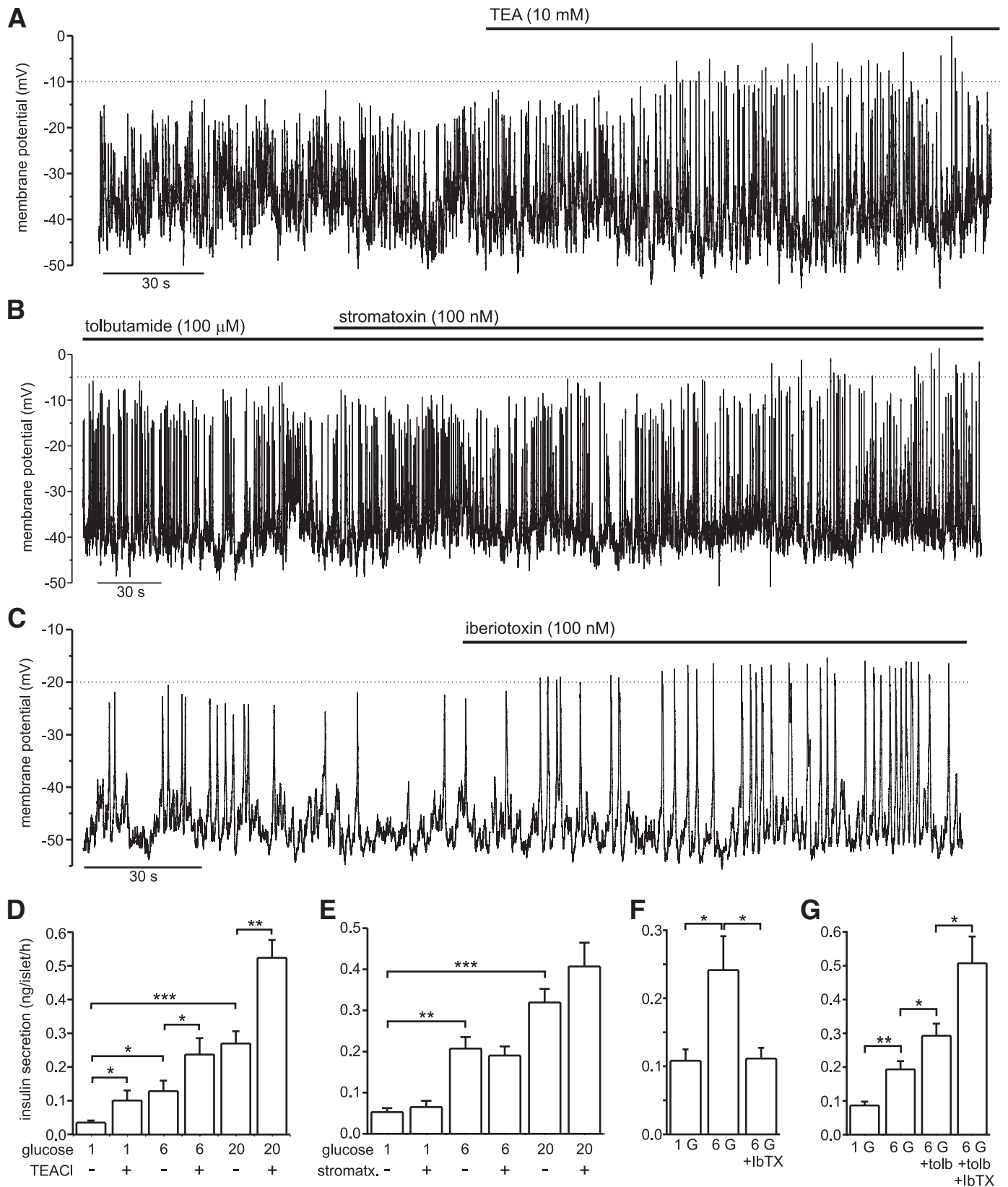


**FIG. 3.** Effects of  $K^+$  channel blockers on  $\beta$ -cell electrical activity and insulin secretion. **A:** Effect of TEA on electrical activity evoked by 6 mmol/l glucose. In this experiment, the action potential peak voltage increased from  $-20 \pm 1$  to  $-13 \pm 1$  mV. **B:** Effect of stromatoxin on electrical activity triggered by 10 mmol/l glucose and 100  $\mu$ mol/l tolbutamide. Spike height in this experiment increased from  $-12 \pm 1$  to  $-8 \pm 1$  mV. **C:** Effect of IbTx on 6 mmol/l glucose-induced electrical activity. Action potentials peaked at  $-22 \pm 1$  and  $-14 \pm 1$  mV before and after addition of IbTx. Dashed horizontal lines have been inserted to facilitate detection of effects on action potential height. **D–G:** Insulin secretion measured at 1, 6, and 20 mmol/l glucose (as indicated) in the absence and presence of 10 mmol/l TEA (**D**), 100 nmol/l stromatoxin (**E**), 100 nmol/l IbTx (**F**), or 100 nmol/l IbTx and/or 0.1 mmol/l tolbutamide (**G**).  $n = 8–9$ . \* $P < 0.05$ ; \*\* $P < 0.01$ ; \*\*\* $P < 0.001$ .

effects of IbTX were observed in current-injection experiments (online appendix Fig. 2A).

Glucose at 6 mmol/l (a concentration attained postprandially in nondiabetic individuals [18]) and 20 mmol/l stimulated insulin secretion 3.7- and 7.7-fold over basal (1 mmol/l), respectively (Fig. 3D). TEA enhanced insulin secretion at 6 and 20 mmol/l glucose by 85 and 94%, respectively (Fig. 3D). By contrast, stromatocin had no significant effects on glucose-induced insulin secretion (Fig. 3E), even when tested at a concentration of 1  $\mu$ mol/l ( $n = 3$  from one donor) (data not shown) (19). We ascertained that stromatocin remained a blocker of the delayed outward current under the experimental conditions used in the secretion assays (i.e., presence of BSA) (data not shown). Whereas IbTX was without effect at 20 mmol/l glucose (data not shown), it abolished the stimulatory effect of 6 mmol/l glucose (Fig. 3F). When tested in the simultaneous presence of 6 mmol/l glucose and 0.1 mmol/l tolbutamide, however, IbTx stimulated insulin secretion by 73% (Fig. 3G).

**Voltage-gated  $\text{Na}^+$  currents.** When the pipettes were filled with a  $\text{Cs}^+$ -containing medium, voltage-clamp depolarizations to 0 mV elicited inward currents consisting of a very transient ( $\sim 2$  ms) and a more slowly inactivating component (Fig. 4A). Whereas the sustained component was suppressed by removal of extracellular  $\text{Ca}^{2+}$  and addition of the broad-spectrum  $\text{Ca}^{2+}$  channel blocker  $\text{Co}^{2+}$ , the transient current was abolished by the selective  $\text{Na}^+$  channel blocker tetrodotoxin (TTX). Voltage-gated  $\text{Na}^+$  currents were activated by depolarizations to  $-30$  mV and above and reached a maximal amplitude of  $40 \pm 7$  pA/pF at 0 mV ( $n = 8$ ) (Fig. 4B and C). The voltage dependence of inactivation was characterized using a two-pulse protocol (Fig. 4D). Inactivation was observed after prepulses positive to  $-80$  mV. A Boltzmann fit yielded values for voltage of half-maximal inactivation ( $V_h$ ) and slope factor ( $n_h$ ) of  $-42 \pm 2$  mV and  $6 \pm 1$  mV ( $n = 9$ ), respectively (Fig. 4E).

We studied the effect of TTX on glucose-induced electrical activity (Fig. 4F). In the presence of 6 mmol/l extracellular glucose, the cell-generated action potentials originating from  $\sim -60$  mV and reaching up to 0 mV. Addition of TTX reversibly reduced the peak voltage of the action potentials from  $-12 \pm 2$  mV to  $-24 \pm 3$  mV ( $n = 2$ ). Similar effects were observed in current injection experiments ( $n = 11$ ) (online appendix Fig. 2B). As shown in Fig. 4G, the TTX-sensitive  $\text{Na}^+$  current is important for glucose-induced insulin secretion, and secretion elicited by 6 and 20 mmol/l glucose was reduced by 70 and 55%, respectively, in the presence of TTX.

**Voltage-gated  $\text{Ca}^{2+}$  currents.**  $\text{Ca}^{2+}$  currents became detectable during depolarizations to  $-50$  mV and peaked at 0 mV (Fig. 5A), where the current density was  $14 \pm 1$  pA/pF ( $n = 41$ ). The activation kinetics of the  $\text{Ca}^{2+}$  current was described using a Hodgkin-Huxley  $m^2$  model. At 0 mV, the current activated with a time constant of  $0.41 \pm 0.02$  ms ( $n = 28$ ). The inactivation of the current was biphasic in most cells. The time constants for the rapid (comprising  $35 \pm 3\%$ ) and slow components ( $43 \pm 3\%$ ) averaged  $6.8 \pm 0.4$  ms ( $n = 25$ ) and  $65 \pm 15$  ms ( $n = 28$ ), respectively.

The  $\text{Ca}^{2+}$  channel subtypes underlying the voltage-gated  $\text{Ca}^{2+}$  current were established using specific blockers. A representative recording is shown in Fig. 5B. In this experiment, the current was reduced by  $>90\%$  by sequential application of first the L-type blocker isradipine alone, followed by a combination of isradipine and the P/Q-type

inhibitor  $\omega$ -agatoxin IVA and finally isradipine together with the T-type antagonist NNC 55-0396 (see also online appendix Fig. 3). Table 1 summarizes the inhibitory effects of the  $\text{Ca}^{2+}$  channel blockers on the peak and integrated  $\text{Ca}^{2+}$  currents evoked by depolarizations from  $-70$  to 0 mV. The cumulative inhibitory effects of isradipine,  $\omega$ -agatoxin IVA, and NNC 55-0396 amounted to 91%. The N-type blocker  $\omega$ -conotoxin GVIA and the R-type blocker SNX-482 exerted negligible effects.

The voltage-dependent inactivation of the T-type  $\text{Ca}^{2+}$  current was studied using a two-pulse protocol (Fig. 5C). The experiments were performed in the presence of isradipine and (in some cells)  $\omega$ -agatoxin IVA to block L- and P/Q-type  $\text{Ca}^{2+}$  currents. A Boltzmann fit to the data points yielded values for  $V_h$  and  $n_h$  of  $-64 \pm 2$  mV and  $8 \pm 1$  mV ( $n = 13$ ), respectively.

The currents flowing through the different channel subtypes were isolated by subtracting the responses recorded after application of the respective blockers from those obtained before blocker application (Fig. 5D). I-V relationships for the total  $\text{Ca}^{2+}$  current and the individual components are shown in Fig. 5E. T-type currents activated at  $-50$  mV and reached a peak between  $-40$  and  $-30$  mV. L-type currents were first seen during depolarizations to  $-40$  mV and reached a maximum between  $-20$  and  $-10$  mV. P/Q-type currents became significant only at potentials beyond  $-20$  mV and peaked at 0 mV. The effect of  $\omega$ -agatoxin IVA showed a slow onset and was maximal only 3–4 min after addition (not shown) (20). Time-dependent rundown of T-type  $\text{Ca}^{2+}$  channels might therefore account for the apparent  $\omega$ -agatoxin sensitivity of a current component at voltages more negative than  $-20$  mV.

In insulin release experiments, isradipine inhibited glucose-stimulated (20 mmol/l) insulin release and reduced secretion below baseline levels (Fig. 6A). By contrast, both SNX-482 and  $\omega$ -conotoxin GVIA were without inhibitory effect, whereas  $\omega$ -agatoxin IVA exerted a moderate inhibitory effect ( $-31\%$ ) (Fig. 6B). The T-type channel blocker NNC 55-0396 was without effect on insulin secretion at 20 mmol/l glucose (not shown). When insulin secretion was evoked by 6 mmol/l glucose, addition of NNC 55-0396,  $\omega$ -agatoxin IVA, and isradipine reduced glucose-stimulated release by 59, 71, and 100%, respectively (Fig. 6C and D), whereas  $\omega$ -conotoxin remained ineffective (not shown).

Figure 6E shows a cell electrically active at 20 mmol/l glucose. In all cells tested, isradipine completely suppressed electrical activity induced by glucose (6 or 20 mmol/l) ( $n = 3$ ) or tolbutamide ( $n = 2$ ). The T-type antagonist NNC 55-0396 also reduced action potential amplitude and frequency (Fig. 6F). The peak voltage attained during the action potential was reduced from  $-28 \pm 2$  mV under control conditions to  $-33 \pm 3$  mV ( $P < 0.05$ ) ( $n = 3$ ) in the presence of NNC 55-0396. Data obtained in membrane potential recordings echo those in the current-injection experiments (online appendix Fig. 2C and D).

**Capacitance measurements.** Capacitance measurements were used to investigate depolarization-evoked exocytosis in human  $\beta$ -cells. While 20-ms depolarizations usually failed to evoke a clear ( $>10$  fF) response, longer depolarization pulses triggered progressively larger capacitance increases (Fig. 7A). In many  $\beta$ -cells, exocytosis continued beyond the depolarization. Figure 7B plots the increase evoked by the depolarization against pulse dura-

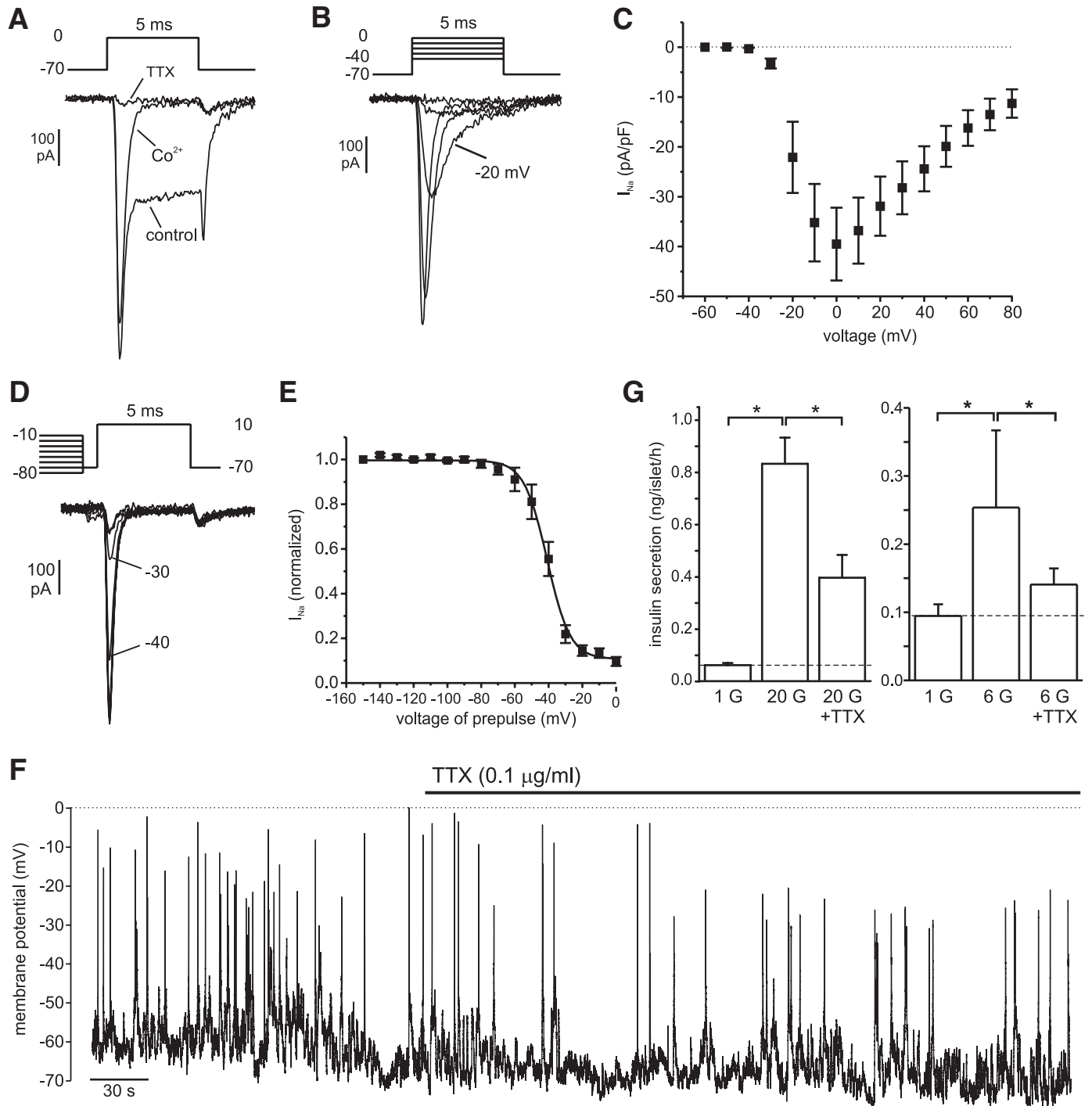


**FIG. 4.** Voltage-gated Na<sup>+</sup> currents. **A:** Inward currents recorded in the presence of TEA (control), after addition of Co<sup>2+</sup> (1 mmol/l) and after additional application of TTX (0.1 μg/ml). **B:** Na<sup>+</sup> currents elicited by depolarizations to voltages between -40 and 0 mV. **C:** I-V relationship for peak Na<sup>+</sup> currents (I<sub>Na</sub>; n = 8). **D:** Na<sup>+</sup> current inactivation. The peak current was measured during a test pulse to +10 mV preceded by a 50-ms conditioning prepulse to different voltages (see schematic above current traces). The responses following prepulses to -40 and -30 mV are indicated by lines. **E:** Steady-state Na<sup>+</sup> current (I<sub>Na</sub>) inactivation measured as in **D** (n = 9). A Boltzmann fit to the data is superimposed. **F:** Effects of TTX (0.1 μg/ml) on electrical activity evoked by 6 mmol/l glucose. Action potentials peaked at -14 ± 2 mV before and -27 ± 1 mV after TTX. Dashed horizontal line has been inserted to facilitate detection of effect on action potential height. **G:** Insulin secretion measured at 1, 6, and 20 mmol/l glucose (1G/6G/20G) with or without TTX (0.1 μg/ml), as indicated (n = 6–8). \*P < 0.05.

tion. The average response during 500-ms depolarizations was 41 ± 5 fF/pF.

Figure 7C shows the relationship between the integrated Ca<sup>2+</sup> current and exocytosis. Exocytosis was small for integrated Ca<sup>2+</sup> currents with a charge of <0.4 pC/pF but then increased supralinearly with charge entry. The relationship was well described by a fourth-order polynomial

function, compatible with cooperative binding of Ca<sup>2+</sup> to the Ca<sup>2+</sup> sensor of exocytosis (21).

We studied the voltage dependence of exocytosis by applying depolarizing pulses from -70 mV to voltages between -40 and +40 mV (Fig. 7D). Depolarizations to -20 mV or below were largely ineffective, but the responses then increased steeply, with a maximum being

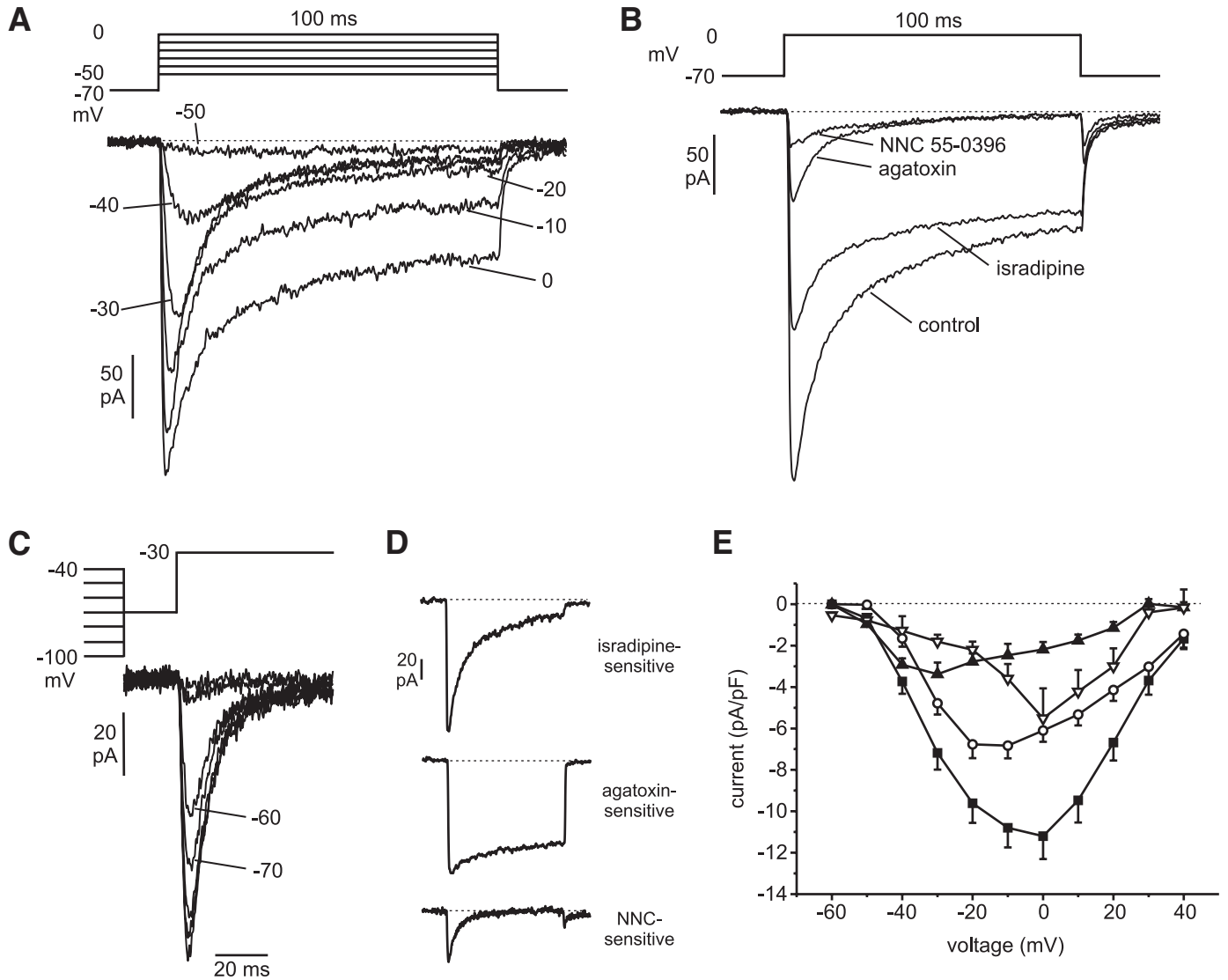


**FIG. 5.** Voltage-gated  $\text{Ca}^{2+}$  currents. **A:**  $\text{Ca}^{2+}$  currents elicited by depolarizations to voltages between  $-50$  and  $0$  mV. **B:** Effect of the sequential application of isradipine ( $10 \mu\text{mol/l}$ ),  $\omega$ -agatoxin IVA ( $200 \text{ nmol/l}$ ), and NNC 55-0396 ( $1 \mu\text{mol/l}$ ). Isradipine was present in all blocker-containing solutions, while  $\omega$ -agatoxin was applied only temporarily as its effects showed no reversibility upon washout. **C:** Steady-state inactivation of T-type  $\text{Ca}^{2+}$  currents measured with a two-pulse protocol, consisting of a test pulse to  $-30$  mV preceded by a  $500$ -ms conditioning pulse to voltages between  $-100$  and  $-40$  mV. The T-type  $\text{Ca}^{2+}$  current was isolated by blocking L- and P/Q-type  $\text{Ca}^{2+}$  currents. The responses obtained after conditioning pulses to  $-70$  and  $-60$  mV are indicated by lines. **D:** L-, P/Q-, and T-type  $\text{Ca}^{2+}$  currents obtained by subtracting currents recorded in the presence of isradipine,  $\omega$ -agatoxin IVA, and NNC 55-0396 from currents observed in the absence of the respective antagonist. **E:** Current-voltage relationship for total  $\text{Ca}^{2+}$  current ( $\blacksquare$ ), L-type ( $\circ$ ) (isradipine sensitive), P/Q-type ( $\nabla$ ) ( $\omega$ -agatoxin sensitive), and T-type ( $\blacktriangle$ ) (NNC 55-0396 sensitive)  $\text{Ca}^{2+}$  currents ( $n = 5$ – $13$ ).

**TABLE 1**  
Effects of  $\text{Ca}^{2+}$  channel blockers on  $\text{Ca}^{2+}$  current charge and peak amplitude

Antagonist	Concentration ( $\mu\text{mol/l}$ )	Inhibition (%)		<i>n</i>
		Charge	Peak current	
Isradipine	10	$38 \pm 3^*$	$49 \pm 3^*$	30
$\omega$ -Agatoxin IVA	0.2	$46 \pm 5^\dagger$	$24 \pm 3^\dagger$	10
NNC 55-0396	1	$6 \pm 1^*$	$18 \pm 2^*$	14
$\omega$ -Conotoxin GVIA	0.1	$2 \pm 3$	$5 \pm 3$	7
SNX-482	0.1	$0 \pm 1$	$4 \pm 1^\dagger$	6

Data are means  $\pm$  SE, unless otherwise indicated.  $\text{Ca}^{2+}$  currents were measured during  $100$ -ms depolarizations from  $-70$  to  $0$  mV. The data are expressed as percent inhibition of control responses ( $*P < 0.001$ ;  $^\dagger P < 0.01$ ).

attained at  $0$  mV and a secondary reduction at more positive voltages. The observed voltage dependence of exocytosis most closely resembles that of the P/Q-type  $\text{Ca}^{2+}$  channels (cf. Figure 5E).

We studied the effects of  $\text{Ca}^{2+}$  channel blockers on depolarization-evoked exocytosis. Whereas  $\omega$ -agatoxin exerted a strong inhibitory action on exocytosis evoked by a  $500$ -ms depolarization to  $0$  mV, the effect of isradipine was weak (Fig. 7E). On average, isradipine and  $\omega$ -agatoxin reduced exocytosis by  $31 \pm 15\%$  (NS) ( $n = 6$ ) and  $80 \pm 3\%$  ( $P < 0.001$ ) ( $n = 5$ ), respectively.

**Expression profiling of human islets.** We quantified mRNA expression of voltage-gated ion channels in nine human islet preparations (online appendix Table 1). All known isoforms of  $\text{Na}^+$  channels were screened. Of the  $\alpha$ -subunits,  $\text{Na}_V1.7$  and  $\text{Na}_V1.6$  dominated, while type  $1\beta$  constitutes  $80\%$  of the total  $\beta$ -subunit expression. Of the

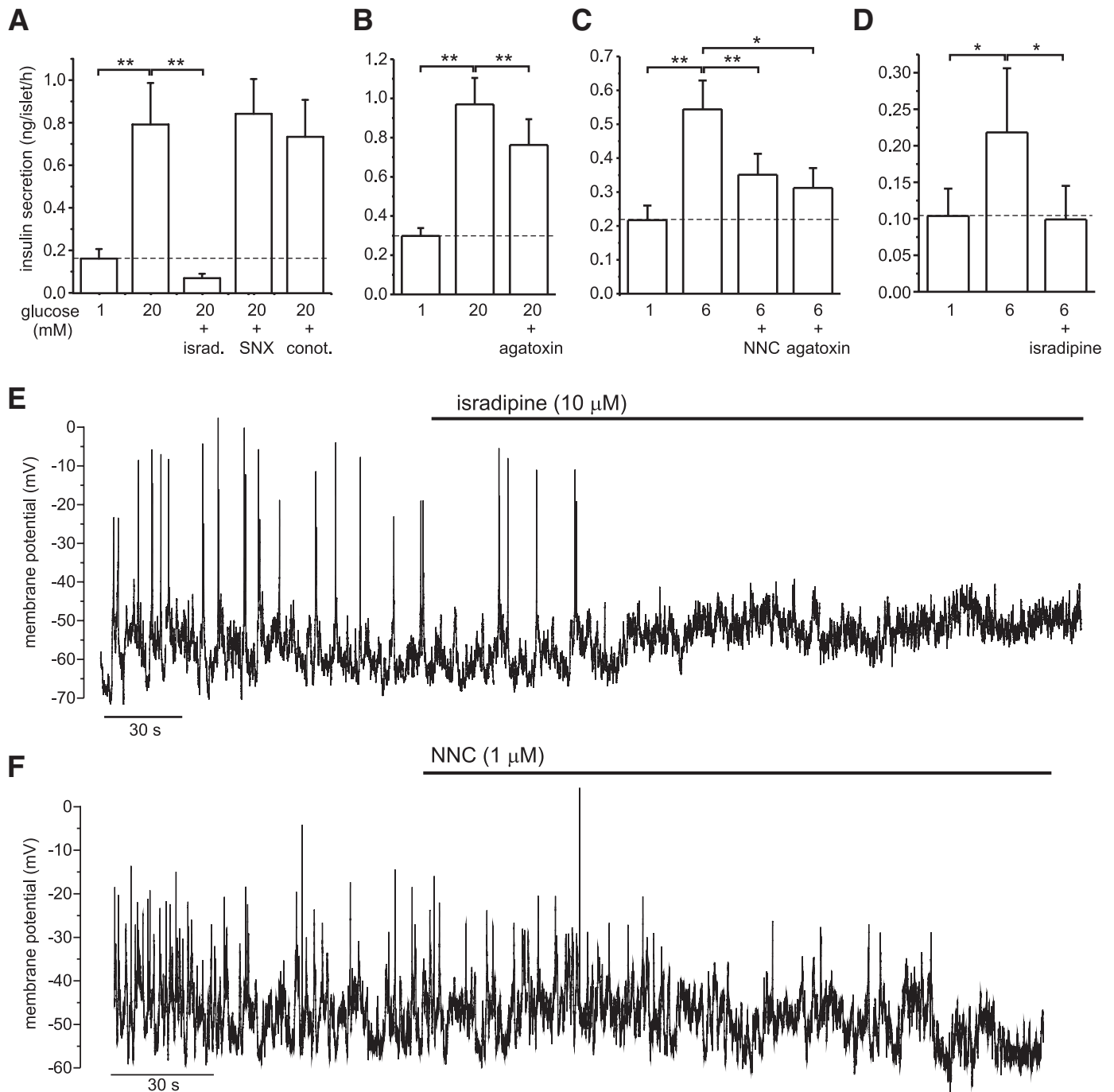


**FIG. 6.** Effects of  $\text{Ca}^{2+}$  channel blockers on insulin secretion and electrical activity. *A–D*: Effects of isradipine (10  $\mu\text{mol/l}$ ), SNX482 (0.1  $\mu\text{mol/l}$ ),  $\omega$ -conotoxin GVIA (0.1  $\mu\text{mol/l}$ ),  $\omega$ -agatoxin IVA (0.2  $\mu\text{mol/l}$ ), and NNC55-0396 (1  $\mu\text{mol/l}$ ) on insulin secretion at the indicated glucose concentrations. *A*:  $n = 9$ ; *B*:  $n = 13$ ; *C*:  $n = 7–9$ ; *D*:  $n = 9$ . \* $P < 0.05$ ; \*\* $P < 0.01$ . *E* and *F*: Effects of isradipine (*E*) and NNC 55-0396 (*F*) on electrical activity elicited by 20 mmol/l glucose (*E*) or 10 mmol/l glucose supplemented with 0.1 mmol/l tolbutamide (*F*).

$\text{Ca}^{2+}$  channels,  $\text{Ca}_v3.2$  ( $\alpha_{1G}$ ; T type),  $\text{Ca}_v1.3$  ( $\alpha_{1D}$ ; L type), and  $\text{Ca}_v2.1$  ( $\alpha_{1A}$ ; P/Q type) isoforms were most abundant and account for 48, 28, and 12% of the transcript numbers, respectively. A selection of voltage-gated  $\text{K}^+$  channels based on Yan et al. (22) was screened. The expression of  $\text{K}_v$  channels was dominated by  $\text{K}_v2.1$  and  $\text{K}_v2.2$  (24 and 73%, respectively). The  $\alpha$ -subunit of the large conductance  $\text{Ca}^{2+}$ -activated  $\text{K}^+$  channels (BK channels) was highly expressed, and of the  $\beta$ -subunits  $\beta_2$  predominated (80%).

## DISCUSSION

We have characterized the voltage-gated membrane currents in identified human  $\beta$ -cells, their molecular composition, and their involvement in exocytosis, electrical activity, and glucose-induced insulin secretion. This was facilitated by the access to novel and selective blockers. Based on these data, we provide a model that outlines the respective roles of the different voltage-gated ion channels in stimulus secretion coupling in human  $\beta$ -cells.



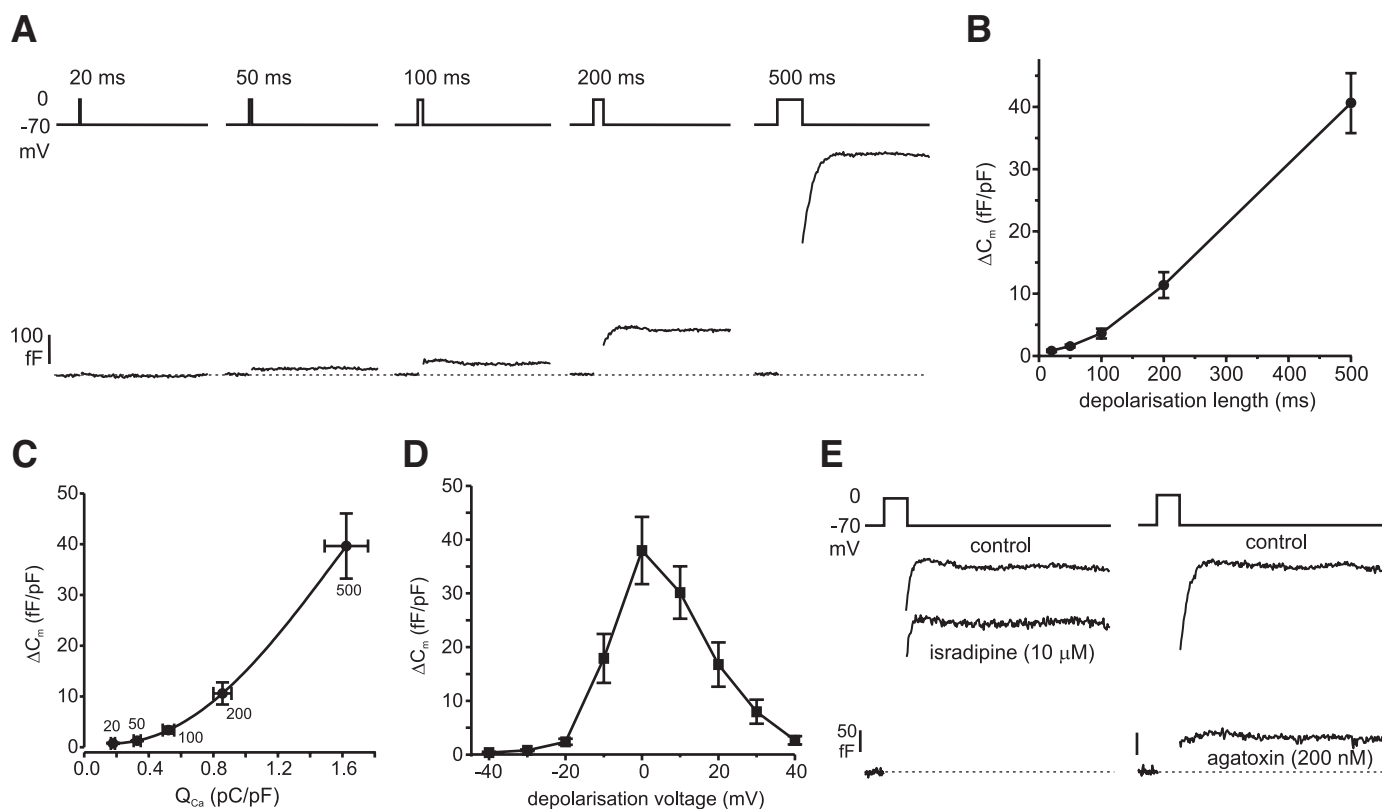


**FIG. 7.** Depolarization-evoked exocytosis. **A:** Capacitance increase evoked by progressively longer depolarizations to 0 mV (applied at 15-s intervals). **B:** Relationship between pulse length and the total (including postpulse response) capacitance increase ( $\Delta C_m$ ). Exocytotic responses have been normalized to cell capacitance ( $n = 16$ ). **C:** Relationship between  $Ca^{2+}$ -current charge ( $Q_{Ca}$ ) and  $\Delta C_m$ , both normalized to cell capacitance ( $n = 12$ ). The numbers next to the symbols indicate the length of the depolarization pulse (ms). The curve was obtained by fitting the data with a fourth-order polynomial function ( $R^2 = 1$ ). **D:**  $\Delta C_m$  (normalized to cell capacitance) in response to 500-ms depolarizations plotted against the voltage during the pulse ( $n = 13$ ). **E:** Effects of isradipine (10  $\mu$ mol/l) and  $\omega$ -agatoxin IVA (200 nmol/l) on depolarization-evoked (500 ms to 0 mV) capacitance increase.

**K<sup>+</sup> currents.** The voltage-gated K<sup>+</sup> current in human  $\beta$ -cells consists of at least two different components. A transient component activates rapidly upon membrane depolarization, is dependent on Ca<sup>2+</sup> influx, and is blocked by IbTX. These properties suggest that it is carried by large-conductance Ca<sup>2+</sup>-activated K<sup>+</sup> channels (BK channels). BK currents exhibited a typical bell-shaped voltage dependence, with decreasing amplitude at potentials >30 mV due to reduced Ca<sup>2+</sup> entry. It can be noted that the peak BK current is observed at a potential ~30 mV more positive than the peak Ca<sup>2+</sup> current (compare Figs. 2D and 5E). This rightward shift reflects both the intrinsic voltage dependence of the channels, with (at fixed Ca<sup>2+</sup> levels) increased open probability at depolarized potentials (23), and the increasing driving force for K<sup>+</sup> entry. Similar to studies in chromaffin cells (24) and mouse  $\beta$ -cells (25), BK currents were recorded despite the presence of a high concentration of EGTA in the intracellular solution. This suggests that BK channels and voltage-gated Ca<sup>2+</sup> channels are closely colocalized (26). In mouse  $\beta$ -cells, BK channels do not play a major role in glucose-induced electrical activity or insulin secretion (27). By contrast, in human  $\beta$ -cells blockade of BK channels increases spike amplitude. In some cells, addition of IbTX suppressed action potential firing. This effect appeared to result from an unexpected ability of IbTX to activate K<sub>ATP</sub> channels, which also accounts for the inhibition of glucose-induced insulin secretion. When insulin secretion was instead measured in the presence of tolbutamide, IbTX, as ex-

pected from the electrophysiological data, stimulated insulin secretion.

The second component of the K<sup>+</sup> current developed with a delayed time course. This component was unaffected by Co<sup>2+</sup> and IbTX but inhibited by stromatoxin and TEA; inhibition by the latter compound was half maximal at ~1 mmol/l. The current is likely to be due to delayed rectifying K<sup>+</sup> channels. K<sub>V2.1</sub> channels, which are dominant in rodent cells (28), are also expressed in human  $\beta$ -cells (22). However, at the mRNA level K<sub>V2.2</sub> channels are more abundant in human islets. In rodent cells, blockade of K<sub>V2.1/2.2</sub> channels stimulates insulin secretion (19,28). By contrast, in human islets the K<sub>V2.1/2.2</sub> blocker stromatoxin had no major effect on insulin release and electrical activity. It has been suggested that human  $\beta$ -cells also express A-type K<sup>+</sup> currents (29), but we have so far detected such currents only in non- $\beta$ -cells in human islets (not shown). Collectively, these data suggest that BK channels are particularly important for spike repolarization. Their activation kinetics and voltage dependence make them ideally suited for this task.

**Na<sup>+</sup> currents.** In agreement with previous studies in human  $\beta$ -cells (10,12), but in marked contrast to mouse  $\beta$ -cells (30–32), the voltage-gated Na<sup>+</sup> current could be activated from physiologically relevant membrane potentials (–70 mV and more positive). Using TTX, we could demonstrate the significance of these channels for action potential generation and insulin secretion. At the mRNA level, human islets express approximately equal amounts

of  $\text{Na}_v1.6$  and  $\text{Na}_v1.7$ . The latter channels are involved in nociception (33), and  $\text{Na}_v1.7$ -specific antagonists are considered as analgesics. The possibility that such channels are involved in insulin secretion suggests that the use of such drugs may cause impaired insulin secretion as a side effect.

**$\text{Ca}^{2+}$  currents and exocytosis.** In agreement with previous studies (5,11), we show that L-type  $\text{Ca}^{2+}$  channels are expressed in human  $\beta$ -cells. Blockade of L-type  $\text{Ca}^{2+}$  channels using the selective antagonist isradipine leads to complete inhibition of glucose-induced insulin secretion. Our data suggest that the importance of L-type channels predominantly results from their essential role in the generation of electrical activity, whereas their role in exocytosis is modest ( $\sim 30\%$ ). The significance of L-type channels for the generation of electrical activity may reflect their voltage dependence: activation commences at voltages as negative as  $-40$  mV (Fig. 5E). The PCR data suggest that the L-type  $\text{Ca}^{2+}$  channel is of the  $\text{Ca}_v1.3$  ( $\alpha 1D$ ) subtype. The fact that the isradipine-sensitive current activates at more negative voltages in human than in mouse  $\beta$ -cells is consistent with this observation (34).

Although expression of P/Q-type  $\text{Ca}^{2+}$  channels in human  $\beta$ -cells has been reported earlier (8), their relative contribution to the total  $\text{Ca}^{2+}$  current and their function in stimulus secretion coupling have been unclear. We now show that P/Q-type  $\text{Ca}^{2+}$  channels account for  $\sim 45\%$  of the integrated whole-cell  $\text{Ca}^{2+}$  current and that they play a critical role in depolarization-evoked exocytosis and glucose-induced insulin secretion, especially at low glucose concentrations (6 mmol/l). At variance with mouse  $\beta$ -cells (35), we found no electrophysiological evidence for the presence of R-type  $\text{Ca}^{2+}$  channels. In fact, they are not at all expressed in human islets (online appendix Table 1).

We further confirm that T-type  $\text{Ca}^{2+}$  channels are also expressed (5) and contribute to electrical activity (10) in human  $\beta$ -cells. Using a recently developed, more selective antagonist (NNC55-9036) (see online appendix Fig. 3), we obtained evidence that T-type channels are involved in insulin release evoked by 6 mmol/l glucose but not by 20 mmol/l glucose. We acknowledge that NNC55-9036 is not ideal in inhibiting non-T-type  $\text{Ca}^{2+}$  currents also. However, the nonspecific effects (unlike those on the T type) were reversible. For secretion studies, islets were therefore preincubated for 15 min with the blocker, followed by a 10-min washout phase. In patch-clamp experiments using the same protocol, only the peak (T-type)  $\text{Ca}^{2+}$  current was significantly reduced after pretreatment with NNC55-9036, whereas the sustained current (non-T type) was unaffected (see legend to online appendix Fig. 3). PCR analysis suggests that the T-type  $\text{Ca}^{2+}$  current in human  $\beta$ -cells is of the  $\text{Ca}_v3.2$  subtype.

**A model for electrical activity in human  $\beta$ -cells.** Based on the findings in the present and previous studies, we propose that at physiological glucose concentrations ( $\sim 6$  mmol/l) the closure of  $\text{K}_{\text{ATP}}$  channel depolarizes the  $\beta$ -cell membrane to potentials above  $-55$  mV. The activation of T-type (at voltages above  $-60$  mV) and L-type  $\text{Ca}^{2+}$  channels (above  $-50$  mV) (Fig. 5E) initiates the action potential. During the upstroke of the action potential, voltage-gated  $\text{Na}^+$  channels also open (above  $-40$  mV) (Fig. 4B and C), leading to a further acceleration of the upstroke and sufficient depolarization to activate P/Q-type  $\text{Ca}^{2+}$  channels (above  $-20$  mV).  $\text{Ca}^{2+}$  influx via P/Q-type (and to a lesser extent L-type)  $\text{Ca}^{2+}$  channels directly triggers exocytosis of insulin granules. The  $\beta$ -cell is repo-

larized by the activation of  $\text{Ca}^{2+}$ -activated BK channels, with  $\text{K}_v2.1/2.2$  channels playing only a minor role. The scenario outlined above is consistent with the observation that the inhibitory actions of TTX (see also 10), NNC55-0936, and  $\omega$ -agatoxin are weaker at 20 than at 6 mmol/l glucose. As shown in Figs. 4F and 6F, inhibition of T-type  $\text{Ca}^{2+}$  channels and  $\text{Na}^+$  channels reduces the action potential amplitude. A reduction of spike height by 15–20 mV (from the normal peak voltage of  $-10$  to 0 mV) will result in  $>50\%$  reduction of both the P/Q-type  $\text{Ca}^{2+}$  current (Fig. 5E) and exocytosis (Fig. 7D). Our data suggest that P/Q-type  $\text{Ca}^{2+}$  channels are more tightly coupled to exocytosis than L-type  $\text{Ca}^{2+}$  channels. Indeed, the exocytotic responses were small during depolarizations to  $-20$  mV, a voltage associated with the maximum activation of the L-type  $\text{Ca}^{2+}$  channels (Fig. 5E).

**Concluding remarks.** It is evident that human and mouse  $\beta$ -cells differ in many respects. Thus, some channels which are not considered functionally important in mouse  $\beta$ -cells (like the BK channels, T- and P/Q-type  $\text{Ca}^{2+}$  channels, and voltage-gated  $\text{Na}^+$  channels) play critical roles in human  $\beta$ -cells. Conversely, R-type  $\text{Ca}^{2+}$  channels and  $\text{K}_v2.1$  channels appear less important in human cells than suggested by previous work in mice. As discussed above, this may have an impact on drug development. It seems unlikely that the differences between human and rodent  $\beta$ -cells are confined to ion channels. Indeed, there are examples of such differences in the literature. Whereas mouse  $\beta$ -cells depend on Glut2 for transmembrane glucose transport, human  $\beta$ -cells instead depend on Glut1 (36). These discrepancies might also be relevant to the understanding of the genetics of type 2 diabetes. Clearly, a gene polymorphism associated with increased risk of type 2 diabetes is more likely to affect insulin secretion if the gene is expressed in human  $\beta$ -cells and vice versa.

#### ACKNOWLEDGMENTS

This work is supported by the Wellcome Trust, the European Union (Biosim [LSHB-CT-2004-005137] and Eurodia [SHM-CT-2006-518153]), and the Department of Health (NIHR Biomedical Research Centres funding scheme).

We thank Dr. S. Hughes, Dr. D. Gray, and Dr. S. Cross for isolation of human islets and D. Wiggins for assistance with hormone release measurements.

#### REFERENCES

- Rorsman P: The pancreatic beta-cell as a fuel sensor: an electrophysiologist's viewpoint. *Diabetologia* 40:487–495, 1997
- Henquin JC, Dufrane D, Nenquin M: Nutrient control of insulin secretion in isolated normal human islets. *Diabetes* 55:3470–3477, 2006
- Tarasov A, Dusonchet J, Ashcroft F: Metabolic regulation of the pancreatic beta-cell ATP-sensitive  $\text{K}^+$  channel: a pas de deux. *Diabetes* 53 (Suppl. 3):S113–S122, 2004
- Ashcroft FM, Rorsman P: Electrophysiology of the pancreatic beta-cell. *Prog Biophys Mol Biol* 54:87–143, 1989
- Davalli AM, Biancardi E, Pollo A, Socci C, Pontiroli AE, Pozza G, Clementi F, Sher E, Carbone E: Dihydropyridine-sensitive and -insensitive voltage-operated calcium channels participate in the control of glucose-induced insulin release from human pancreatic beta cells. *J Endocrinol* 150:195–203, 1996
- Kelly RP, Sutton R, Ashcroft FM: Voltage-activated calcium and potassium currents in human pancreatic beta-cells. *J Physiol* 443:175–192, 1991
- Pollo A, Lovallo M, Biancardi E, Sher E, Socci C, Carbone E: Sensitivity to dihydropyridines, omega-conotoxin and noradrenaline reveals multiple high-voltage-activated  $\text{Ca}^{2+}$  channels in rat insulinoma and human pancreatic beta-cells. *Pflugers Arch* 423:462–471, 1993
- Sher E, Giovannini F, Codignola A, Passafaro M, Giorgi-Rossi P, Volsen S, Craig P, Davalli A, Carrera P: Voltage-operated calcium channel heteroge-

- neity in pancreatic beta cells: physiopathological implications. *J Bioenerg Biomembr* 35:687–696, 2003
9. Cabrera O, Berman DM, Kenyon NS, Ricordi C, Berggren PO, Caicedo A: The unique cytoarchitecture of human pancreatic islets has implications for islet cell function. *Proc Natl Acad Sci U S A* 103:2334–2339, 2006
  10. Barnett DW, Pressel DM, Misler S: Voltage-dependent Na<sup>+</sup> and Ca<sup>2+</sup> currents in human pancreatic islet beta-cells: evidence for roles in the generation of action potentials and insulin secretion. *Pflugers Arch* 431: 272–282, 1995
  11. Misler S, Barnett DW, Pressel DM, Gillis KD, Scharp DW, Falke LC: Stimulus-secretion coupling in  $\beta$ -cells of transplantable human islets of Langerhans: evidence for a critical role for Ca<sup>2+</sup> entry. *Diabetes* 41:662–670, 1992
  12. Pressel DM, Misler S: Sodium channels contribute to action potential generation in canine and human pancreatic islet B cells. *J Membr Biol* 116:273–280, 1990
  13. Gopel SO, Kanno T, Barg S, Rorsman P: Patch-clamp characterisation of somatostatin-secreting-cells in intact mouse pancreatic islets. *J Physiol* 528:497–507, 2000
  14. Gopel SO, Kanno T, Barg S, Weng XG, Gromada J, Rorsman P: Regulation of glucagon release in mouse cells by KATP channels and inactivation of TTX-sensitive Na<sup>+</sup> channels. *J Physiol* 528:509–520, 2000
  15. Macdonald PE, Marinis YZ, Ramracheya R, Salehi A, Ma X, Johnson PR, Cox R, Eliasson L, Rorsman P: A KATP channel-dependent pathway within alpha cells regulates glucagon release from both rodent and human islets of Langerhans. *PLoS Biol* 5:e143, 2007
  16. Braun M, Wendt A, Buschard K, Salehi A, Sewing S, Gromada J, Rorsman P: GABAB receptor activation inhibits exocytosis in rat pancreatic beta-cells by G-protein-dependent activation of calcineurin. *J Physiol* 559:397–409, 2004
  17. Zhang Q, Bengtsson M, Partridge C, Salehi A, Braun M, Cox R, Eliasson L, Johnson PR, Renstrom E, Schneider T, Berggren PO, Gopel S, Ashcroft FM, Rorsman P: R-type Ca(2+)-channel-evoked CICR regulates glucose-induced somatostatin secretion. *Nat Cell Biol* 9:453–460, 2007
  18. Kruszynska YT: Physiology of fuel homeostasis. In *Textbook of Diabetes*. 2nd ed. Pickup J, Williams G, Eds. Oxford, Blackwell Science, 1997, p. 11–13
  19. Herrington J, Zhou YP, Bugianesi RM, Dulski PM, Feng Y, Warren VA, Smith MM, Kohler MG, Garsky VM, Sanchez M, Wagner M, Raphaelli K, Banerjee P, Ahaghotu C, Wunderler D, Priest BT, Mehl JT, Garcia ML, McManus OB, Kaczorowski GJ, Slaughter RS: Blockers of the delayed-rectifier potassium current in pancreatic  $\beta$ -cells enhance glucose-dependent insulin secretion. *Diabetes* 55:1034–1042, 2006
  20. Ligon B, Boyd III AE, Dunlap K: Class A calcium channel variants in pancreatic islets and their role in insulin secretion. *J Biol Chem* 273:13905–13911, 1998
  21. Heinemann C, Chow RH, Neher E, Zucker RS: Kinetics of the secretory response in bovine chromaffin cells following flash photolysis of caged Ca<sup>2+</sup>. *Biophys J* 67:2546–2557, 1994
  22. Yan L, Figueroa DJ, Austin CP, Liu Y, Bugianesi RM, Slaughter RS, Kaczorowski GJ, Kohler MG: Expression of voltage-gated potassium channels in human and rhesus pancreatic islets. *Diabetes* 53:597–607, 2004
  23. Barrett JN, Magleby KL, Pallotta BS: Properties of single calcium-activated potassium channels in cultured rat muscle. *J Physiol* 331:211–230, 1982
  24. Marty A, Neher E: Potassium channels in cultured bovine adrenal chromaffin cells. *J Physiol* 367:117–141, 1985
  25. Smith PA, Bokvist K, Arkhammar P, Berggren PO, Rorsman P: Delayed rectifying and calcium-activated K<sup>+</sup> channels and their significance for action potential repolarization in mouse pancreatic beta-cells. *J Gen Physiol* 95:1041–1059, 1990
  26. Berkefeld H, Sailer CA, Bildl W, Rohde V, Thumfart JO, Eble S, Klugbauer N, Reisinger E, Bischofberger J, Oliver D, Knaus HG, Schulte U, Fakler B: BKCa-Cav channel complexes mediate rapid and localized Ca<sup>2+</sup>-activated K<sup>+</sup> signaling. *Science* 314:615–620, 2006
  27. Kukuljan M, Goncalves AA, Atwater I: Charybdotoxin-sensitive K(Ca) channel is not involved in glucose-induced electrical activity in pancreatic beta-cells. *J Membr Biol* 119:187–195, 1991
  28. MacDonald PE, Sewing S, Wang J, Joseph JW, Smukler SR, Sakellaropoulos G, Wang J, Saleh MC, Chan CB, Tsushima RG, Salapatek AM, Wheeler MB: Inhibition of Kv2.1 voltage-dependent K<sup>+</sup> channels in pancreatic beta-cells enhances glucose-dependent insulin secretion. *J Biol Chem* 277:44938–44945, 2002
  29. Herrington J, Sanchez M, Wunderler D, Yan L, Bugianesi RM, Dick IE, Clark SA, Brochu RM, Priest BT, Kohler MG, McManus OB: Biophysical and pharmacological properties of the voltage-gated potassium current of human pancreatic beta-cells. *J Physiol* 567:159–175, 2005
  30. Göpel S, Kanno T, Barg S, Galvanovskis J, Rorsman P: Voltage-gated and resting membrane currents recorded from B-cells in intact mouse pancreatic islets. *J Physiol* 521 Pt 3:717–728, 1999
  31. Leung YM, Ahmed I, Sheu L, Tsushima RG, Diamant NE, Hara M, Gaisano HY: Electrophysiological characterization of pancreatic islet cells in the mouse insulin promoter-green fluorescent protein mouse. *Endocrinology* 146:4766–4775, 2005
  32. Plant TD: Na<sup>+</sup> currents in cultured mouse pancreatic B-cells. *Pflugers Arch* 411:429–435, 1988
  33. Cox JJ, Reimann F, Nicholas AK, Thornton G, Roberts E, Springell K, Karbani G, Jafri H, Mannan J, Raashid Y, Al-Gazali L, Hamamy H, Valente EM, Gorman S, Williams R, McHale DP, Wood JN, Gribble FM, Woods CG: An SCN9A channelopathy causes congenital inability to experience pain. *Nature* 444:894–898, 2006
  34. Koschak A, Reimer D, Huber I, Grabner M, Glossmann H, Engel J, Striessnig J: alpha 1D (Cav1.3) subunits can form l-type Ca<sup>2+</sup> channels activating at negative voltages. *J Biol Chem* 276:22100–22106, 2001
  35. Jing X, Li DQ, Olofsson CS, Salehi A, Surve VV, Caballero J, Ivarsson R, Lundquist I, Pereverzev A, Schneider T, Rorsman P, Renstrom E: CaV2.3 calcium channels control second-phase insulin release. *J Clin Invest* 115:146–154, 2005
  36. De Vos A, Heimberg H, Quartier E, Huypens P, Bouwens L, Pipeleers D, Schuit F: Human and rat beta cells differ in glucose transporter but not in glucokinase gene expression. *J Clin Invest* 96:2489–2495, 1995